# Deflated Carbon Nanospheres Encapsulating Tin Cores Decorated on Layered 3-D Carbon Structures for Low-Cost Sodium Ion Batteries

Wei Chen and Da Deng*

Department of Chemical Engineering and Materials Science, Wayne State University, Detroit, Michigan 48202, United States

S *Supporting Information*

ABSTRACT: Novel deflated carbon nanospheres encapsulating metallic tin cores were successfully synthesized and decorated on 3-D layered carbon with wall-like structures. The composite was synthesized by facile *in situ* carbonization of walnut shell membranes and chemical vapor deposition (CVD) and can be used as negative electrodes for sodium ion batteries. The *in situ* reduction of SnO_2 particles to metallic Sn particles could induce volumetric shrinkage of the particles due to the density difference. The encapsulation of Sn particles by carbon nanospheres under CVD conditions can form unique deflated Sn@C nanoparticles firmly attached on the surface of the 3-D carbon derived from a typical agricultural waste. Particularly interesting, all the carbon nanospheres are in deflated spherical shape, which could provide extra space for volume expansion during charging in Na insertion into the enclosed Sn. The as-prepared composite in the form of pieces of materials are ready electrodes that can be directly assembled into batteries without any further treatment, in contrast to the conventional multiple-step procedure in making electrodes. Preliminary results demonstrated the potential application of the as-prepared deflated Sn@C nanospheres on 3-D carbon in future sodium ion batteries. Impressive high Coulombic efficiencies were achieved at different currents in SIBs. It should be noted that we observed significant differences in the electrochemical performances of the as-prepared deflated Sn@C nanospheres on 3-D carbon in reversible Na and Li storage. Deflated carbon nanospheres would be broken during cycling in Na storage but were well preserved in Li storage. Those observations suggest the importance of the ionic size of Li and Na and their effects on the electrode materials during charge–discharge cycling.
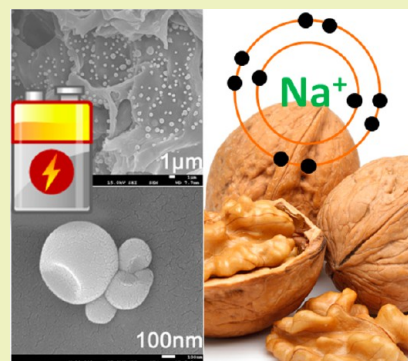
KEYWORDS: *Deflated nanosphere, Carbonization, Sn@C, CVD, Sodium ion batteries, Biomass, Carbonization, in situ reduction*

■ INTRODUCTION

Rechargeable batteries for energy storage have attracted much attention in the past decades. Since the first commercialization of rechargeable lithium-ion batteries (LIBs) by Sony in 1991, LIBs have been considered the powerhouse for current revolution of personal mobile electronic devices. LIBs are playing increasing roles in the emerging market of electric vehicles and energy storage for green grids. The Foreign Policy magazine even published an article entitled "The Great Battery Race" to highlight the worldwide interest in batteries.[1] It is expected that 100 gigawatt hours of LIBs are required to meet the demands by 2018.[2] The long-term "stock" goal of having 1 billion 40 kW h LIBs for electric vehicles will make it a tremendous challenge for the global lithium reserves to meet the requirement for lithium.[3] There are two main issues associated with LIBs for future applications: (1) high cost in the short term and (2) limited lithium reserves in the long term. In fact, the price of Li_2CO_3 was in a steep rise during the past decade.[4] With respect to large-scale stationary energy storage systems for energy grids in sustainable energy networks of wind and solar energy, next generation low-cost rechargeable batteries must be developed. Sodium ion batteries (SIBs), as potential LIB alternatives, are expected to be produced at a lower cost than that of LIBs in the future.[5−8] Mass-produced

SIBs with comparable performances as LIBs will have a significant impact on the environment and society.[4] Additionally, due to the lower standard half-reaction potential of sodium (2.714 V for Na/Na^+) as compared to that of lithium (3.045 V for Li/Li^+), electrolyte degradation will be reduced, and a safe electrolyte with low decomposition potential can be used in SIBs to enhance safety.[9] In other words, not only are SIBs low cost, but they are also good candidates to replace LIBs as safer rechargeable batteries.

The performances of the highly attractive reemerging SIBs will be strongly dependent on electrode materials that are developed.[3,10−13] A number of electrode materials have been explored.[11] For example, cathode materials, such as carbon-coated $NaVPO_4F$, could deliver a reversible capacity of 98 mA h g^{-1}.[14] Other options include $Na_{0.44}MnO_2$ particles that delivered 65 mA h g^{-1},[15] $Na_xCo[Fe(CN)_6]_{0.90}2.9H_2O$ that delivered 135 mA h g^{-1},[16] layered $Na_{0.71}CoO_2$ that delivered 80 mA h g^{-1},[17] $KFe_{(II)}Fe_{(III)}(CN)_6$ that delivered 100 mA h g^{-1},[18] and Na_2FePO_4F that exhibited high voltage of 3.5 V.[6] In terms of anode materials, the widely used graphite in LIBs, however,

cannot reversibly store a significant amount of Na, typically less than 5 mA h g^{-1} due to lack of Na intercalation.[3,4,19,20] On the other hand, disordered nongraphitic carbons can reversibly store more Na as compared to graphite.[3,4] Carbon nanowires prepared by pyrolyzation of polyaniline demonstrated impressive performance in Na storage.[21] Nanocellular carbon foams delivered 152 mA h g^{-1}.[22] Furthermore, metals, metal oxides, and phosphorus have been investigated as anode materials as well.[23−32]

In particular metallic Sn has been demonstrated to be a promising anode material for SIBs.[27−30,33−37] The theoretical capacity of Sn, based on the alloying/dealloying mechanism, is 847 mA h g^{-1} (Na$_{15}$Sn$_4$). This is more than two times higher than the carbon anode in LIBs, based on the intercalation/deintercalation mechanism of 372 mA h g^{-1} (LiC$_6$). However, metallic Sn has a very poor cycling performance with dramatic capacity loss in a few cycles due to the issue of pulverization. The volumetric expansion due to electrochemical sodiation could be as high as 420% (Na$_{15}$Sn$_4$).[38] To overcome this problem, a number of strategies, such as alloying with Sb and mixing with carbon, have been explored.[27,28,31,34,39,40] It would be ideal to encapsulate Sn in a confined volume with enough space for volume expansion during Na insertion to avoid pulverization. Generally, it is more convenient to prepare SnO$_2$ nanoparticles than metallic Sn nanoparticles. Additionally, SnO$_2$ can be reduced to metallic Sn by hydrocarbon. On the other hand, many biomasses can be easily carbonized by hydrothermal methods or calcination under an inert atmosphere to achieve carbon with unique structures,[41−43] which could be suitable to support Sn nanoparticles.

Herein, we report a facile method for *in situ* (1) carbonization of biomass of walnut shell membranes with unique inherited 3-D structure under high temperature, (2) carbothermic reduction of SnO$_2$ to Sn nanoparticles by chemical vapor deposition (CVD) of acetylene, and (3) encapsulation of Sn particles by carbon nanospheres through deposition of carbon from CVD. It is interesting to highlight that all the carbon nanospheres encapsulating metallic Sn are in a deflated spherical shape, which could provide additional space for Sn to expand. The Sn@C deflated spheres are uniformly and firmly attached on the layered carbon from carbonized walnut shell membranes. As the final products are pieces of materials, they are ready electrodes that can be directly assembled into testing cells without any further treatment. We observed significant differences in electrochemical performances of the as-prepared composite in the reversible storage of Na and Li. Sn@C nanospheres would be broken in SIBs but well preserved in LIBs even at higher current rates after 100 cycles.

EXPERIMENTAL SECTION

Materials Preparation. The raw walnut shell membranes were mechanically peeled off from the inner side of the freshly opened dry walnut shells. Pieces of walnut shell membranes were mixed with 0.1 mL SnCl$_4$ in 30 mL water under stirring for 48 h. The solution turned to milky in color indicating hydrolysis of SnCl$_4$. The treated walnut shell membranes were collected and washed by ethanol and dried in a vacuum oven overnight to obtain membranes deposited with xerogel. The samples were then put in a crucible and transferred to a tube furnace for *in situ* thermal carbonization and CVD process. Typically, the process was carried out at a temperature of 650 °C under a flow of 10% C$_2$H$_2$ balanced by 90% Ar at a rate of 30 standard cubic centimeter per minute (sccm) for 3 h. The heating rate was set at 20 °C/min, and the tube furnace was purged with pure Ar for about 1 h

to eliminate oxygen inside. C$_2$H$_2$ gas was switched on only during the CVD process, and the system was cooled under Ar.

Materials Characterization. Powder X-ray diffraction (XRD) was carried out with a Rigaku Smartlab X-ray diffractometer using Cu Kα radiation (λ = 0.15418 nm). The morphologies of the products were characterized by a field emission/scanning electron microscopy (JSM-6510LV SEM and JSM-7600 FESEM equipped with X-ray energy-dispersive spectrometer (EDS)), and by transmission electron microscopy (JEOL 2010 TEM) with an accelerating voltage of 200 kV.

Electrochemical Measurements. Pieces of the as-prepared composite were directly assembled into Swagelok-type cells without any treatment. The piece of composite as the working electrode was coupled with a metallic sodium foil as the counter electrode, 1 M solution of NaClO$_4$ in a 50:50 v/v mixture of ethylene carbonate (EC) and diethyl carbonate (DEC) as the electrolyte, and a polypropylene membrane (Celgard 3501) as the separator. They were charged and discharged galvanostatically at room temperature in the voltage window of 0.005−2 V at different rates on a MTI BST8-WA battery tester.

RESULTS AND DISCUSSION

The schematic of the experimental procedure illustrating the changes in compositions in each step is shown in Figure 1. As a
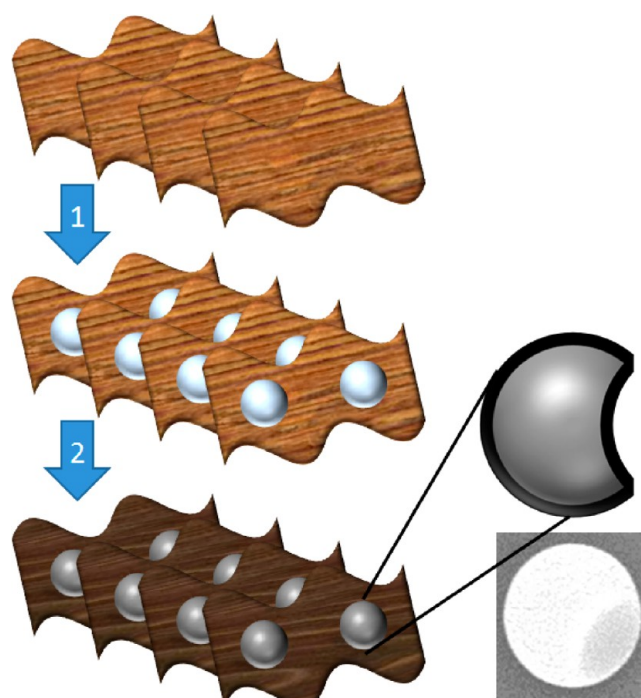

Figure 1. Schematic of experimental procedure showing the changes in material composition in each step. The zoom-in illustration of the unique Sn@C deflated sphere is shown on the upper right side. A typical FESEM image of such a deflated nanosphere is shown on the lower right side.

typical biomass, walnut shell membranes were selected from a side discovery on the carbonization of walnut shells. We realized that the walnut shell membrane just close to the inner section of the endocarp has a unique 3-D porous structure at microscale and could be collected by peeling off pieces of materials (Figure 2 and Figure S1, Supporting Information). In the first step, walnut shell membranes were coated with SnO$_2$ nanoparticles obtained from heating coated xerogel from the hydrolysis of SnCl$_4$. The hydrolysis of SnCl$_4$ into SnO$_2$ nanoparticles is well documented.[44] The surface of the 3-D
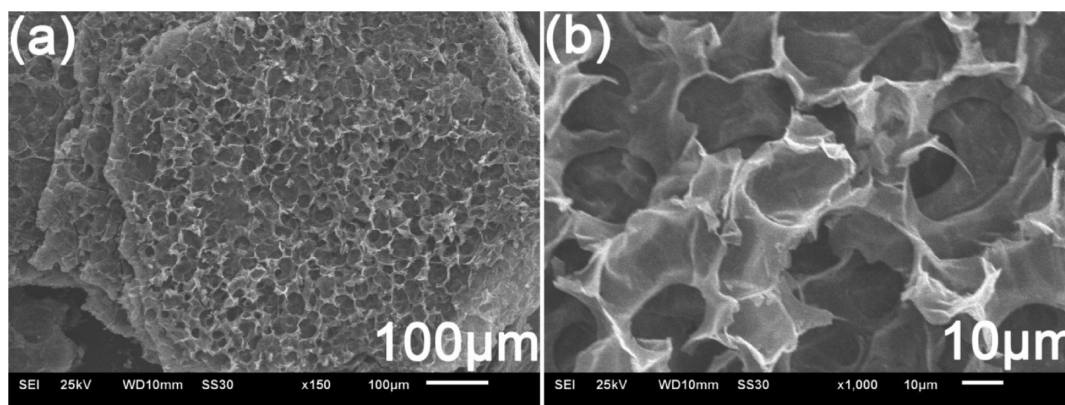
Figure 2. SEM images of a walnut membrane carbonized at 650 °C for 3 h in Ar: (a) low magnification overall view and (b) zoom-in view showing the detailed 3-D layered structures.

walnut shell membrane, similar to other biomass, is covered with −OH or =C=O groups and therefore is hydrophilic. This hydrophilic surface and 3-D structure facilitate the coating of SnO_2 nanoparticles on the surface. In the second step, the decomposing of acetylene under CVD conditions could reduce SnO_2 nanoparticles to metallic Sn and *in situ* form a carbon shell to encapsulate the metallic Sn particles forming Sn@C nanospheres.

Acetylene plays multiple roles here: (1) as a reducing agent to reduce SnO_2 to metallic Sn, (2) as a carbon source to coat Sn with a carbon sheath, and (3) as a protecting gas to avoid oxidization of the walnut shell membrane under high temperature. The reduction of SnO_2 to metallic Sn by acetylene is well documented.[45−47] The 3-D structure of the walnut shell membrane provides channels for acetylene gas to diffuse through the materials and allows CVD to occur locally. At the same time, the walnut shell membrane is carbonized under high temperature, similar to carbonization of other biomass under an inert atmosphere.[48] Due to the density difference between SnO_2 and metallic Sn, the carbon spheres will be deflated as a result of volume shrinking when the enclosed SnO_2 nanoparticle was reduced to Sn. Consequently, unique deflated Sn@C nanospheres-decorated 3-D carbon structures are formed as shown in the enlarged particle in Figure 1.

The successful reduction of SnO_2 to metallic Sn is evidenced by XRD (Figure 3). The XRD pattern (black) of the pristine carbonized walnut shell membrane has no distinguishable peaks indicating that the carbon converted from the biomass is mainly nongraphitized carbon due to carbonization at low temperature (650 °C). After CVD treatment, sharp diffraction peaks are observed (blue) that can be assigned to β-metallic Sn with a tetragonal structure (JCPDS card no. 04-0673). Meanwhile, weak peaks of SnO_2 are still visible that could be attributed to the incomplete reduction of SnO_2 nanoparticles or a trace amount of SnO_2 that could be trapped inside the 3-D structure and might not be exposed for CVD. TGA analysis shows that the metallic tin is about 8.3% by weight in the composite (Figure S2, Supporting Information). We are in the process of optimizing and increasing the amount of tin loaded, and the results will be published once available.

The distribution of deflated Sn@C nanospheres on the 3-D structures is uniform through all the accessible surface of the 3-D walnut shell membrane, as evidenced by the low-magnification FESEM image (Figure 4a). Due to the 3-D porous structure, the walnut shell membrane provides multiple
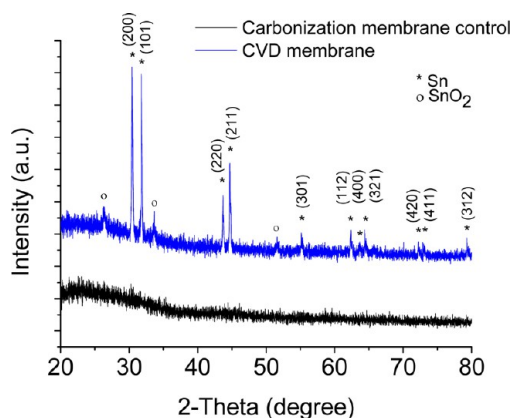

Figure 3. XRD characterization of the (black) pristine carbonized walnut shell membrane and (blue) Sn@C deflated nanosphere on 3-D carbon formed by *in situ* walnut membrane carbonization, SnO_2 carbon thermal reduction to metallic Sn, and encapsulation forming Sn@C nanoparticles. All main peaks can be assigned to metallic Sn.

sites for Sn@C nanoparticles to attach. The zoom-in view more clearly shows that the Sn@C nanoparticles are deposited on both sides of the layered carbon of the carbonized 3-D biomass and distributed evenly (Figure 4b). The particles are attached on the layered carbon firmly. Even for those parts of tilted or standing layered carbon, the Sn@C nanospheres are attached. In fact, mechanical vibration and repeatedly applying vacuum during sample preparation did not affect the attachment. Attempts to isolate deflated Sn@C nanospheres by brief ultrasonication for TEM characterization were not successful, which further indicates good attachment. The mechanical robustness could be attributed the C−C bonds formed between carbon deposited on the surface of layered carbon and the carbon sheath wrapping the Sn particles. The carbon could be deposited from the locally catalytically decomposed acetylene, which can enhance the integration between the particle and the substrate. A few typical Sn@C nanoparticles are shown in Figure 4c. They are in the size of 100−1000 nm. It is particularly interesting to highlight that all Sn@C nanoparticles are unique in the way that each particle regardless of its size is nonspherical or deflated spherical in morphology. The different appearance in terms of degree of deflation observed is due to the different sitting orientations. Four nanoparticles aggregated on the surface of the carbonized walnut shell membrane more clearly illustrate the deflation in each particle and their different
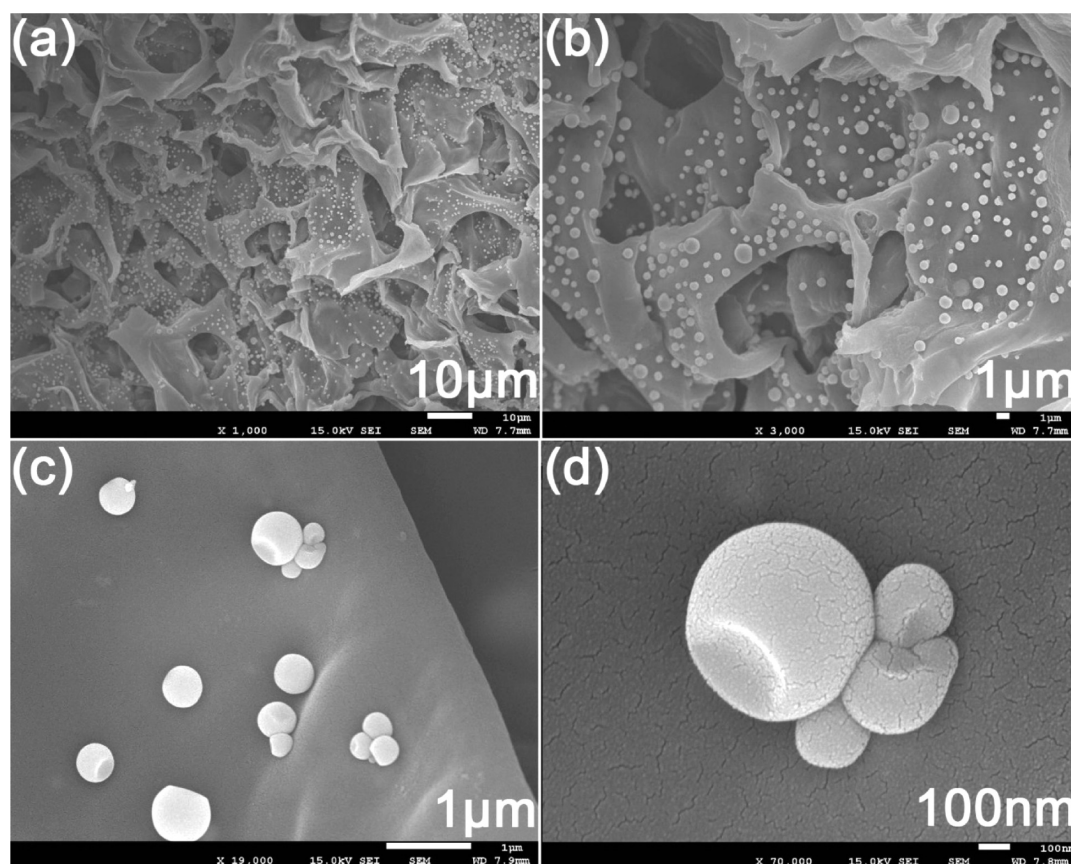
Figure 4. FESEM characterization of the Sn@C deflated nanosphere on 3-D carbon formed by *in situ* carbonization of walnut membranes and CVD reduction of SnO$_2$: (a) low-magnification overall view, (b) zoom-in view showing distribution of the deflated Sn@C nanospheres on both sides of the layered carbon, (c) zoom-in view of a few representative Sn@C nanospheres on the surface of the walnut membrane-based carbon clearly showing the deflated shapes, and (d) high-magnification view of a few aggregated Sn@C nanospheres with deflated carbon spheres.
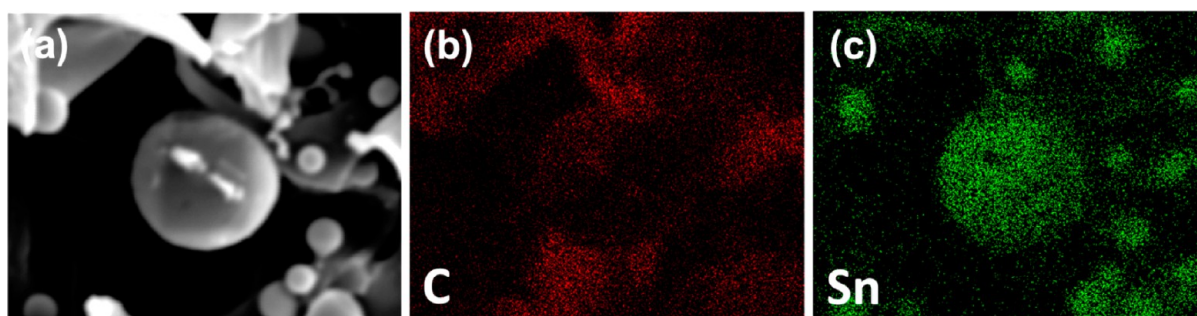

Figure 5. Elemental mapping analysis of the Sn@C deflated nanosphere on 3-D carbon: (a) SEM image of a few representative Sn@C nanospheres on layered carbon, (b) carbon, and (c) tin elemental distribution in the correspond SEM image in panel a. Experimental conditions: 800 °C and 10% C$_2$H$_2$/90% Ar at a flow rate of 65 sccm for 3h.

orientations from the surface of the layered carbon as observed by high-magnification FESEM (Figure 4d).

The effects of experimental parameters on the products were also explored. When the CVD temperature was set at 800 °C instead of 650 °C, similar Sn@C nanoparticles were formed on the layered carbon from walnut shell membranes (Figure S4a and b, Supporting Information). It is interesting to note that the size distribution is broad, and particles of a few micrometers were observed. When both the amount of SnO$_2$ nanoparticles coating and CVD flow rate were increased, Sn@C nanospheres were distributed on the 3-D carbon at a much high density. Additionally, Sn@C nanospheres with multiple points of deflation were observed as highlighted by the red boxes in

Figure S4c and d of the Supporting Information. The multiple points of deflation in the Sn@C nanosphere on 3-D carbon are observed in samples prepared from precursor solutions of different concentrations of SnCl$_4$ as well (Figure S5, Supporting Information). Those observations suggest that it would be possible to tune the degree of deflation on the carbon nanospheres and density of distribution by adjusting experimental conditions, which is our ongoing effort.

The carbon sheath and enclosed metallic Sn nanoparticles are further characterized by elemental mapping analysis (Figure 5) and TEM (Figure 6). The SEM images of a few typical Sn@C nanospheres on walnut shell membrane-based carbon selected for elemental mapping analysis is shown in Figure
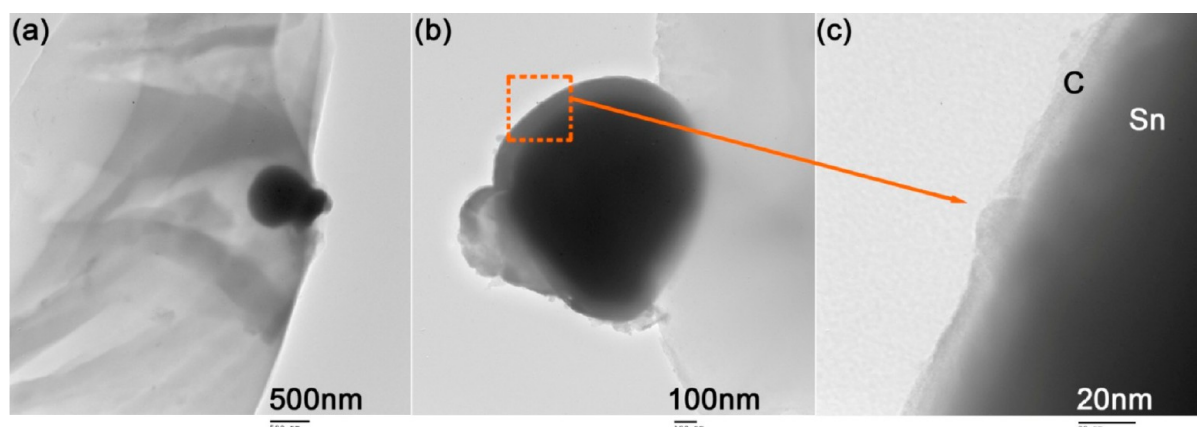
Figure 6. TEM images of deflated Sn@C nanospheres-decorated layered carbon: (a) low-magnification view of the light contrast layered carbon from the carbonized walnut membrane and dark contrast Sn@C nanosphere, (b) representative Sn@C nanosphere with a carbon shell and metallic Sn core more clearly visible with sharp contrast under TEM, and (c) high-magnification TEM of a section in panel b showing that the thickness of the carbon shell is about 9 nm.

5a, where both the Sn@C nanoparticles and the layered carbon from walnut shell membrane were analyzed. The corresponding carbon distribution (Figure 5b) suggested that the main carbon content is from 3-D structure of carbonized walnut shell membrane. The thin carbon shell from the Sn@C nanosphere forming a curved boundary line is still weakly observed. This elemental distribution pattern suggests that the carbon shell is formed on the surface of the nanoparticles. The corresponding tin elemental distribution (Figure 5c) clearly duplicates the outlines of the nanospheres observed in SEM image (Figure 5a). This provides solid evidence that the Sn nanoparticle is wrapped by a carbon sheath. Nanospheres in different samples prepared under different conditions discussed previously were confirmed be to Sn@C sheath−core structure.

A low-magnification TEM image (Figure 6a) clearly reveals a typical nonspherical Sn@C nanosphere decorated on layered carbon from a carbonized walnut shell membrane. A high-magnification TEM image of another typical nonspherical Sn@C nanosphere shows that there is an obvious color contrast between the dark central particle and light coating shell (Figure 6b). This provides more evidence of a deflated Sn@C core−sheath nanospherical structure. The structure is more clearly revealed by the zoom-in high-magnification view (Figure 6c). Additional TEM characterizations of the Sn@C nanospheres clearly show the space between the carbon sheath and the tin core and the nonspherical shape (Figure S3a, Supporting Information). The HRTEM image shows the carbon sheath is polycrystalline with short-range graphene layers aligned outside of the metallic tin core, and SAED determined that the core is crystalline metallic Sn (Figure S3b, Supporting Information). The thickness of the carbon shell is about 9−12 nm. The polycrystalline features in the carbon sheaths were observed in other Sn-assisted catalytic decompositions of acetylene-by.[45−47,49,50] The relative intensity of D and G bands (I_D/I_G) from Raman spectra, corresponding to the degree of disordered carbon, is typically in the range between 0.85 and 1.3.[50,51] The low degree of graphitization of the carbon sheath could be due to the low temperature of 650 °C used in CVD.[45−47] Under TEM survey, all the deflated Sn@C nanospheres were attached on the layered carbon from the walnut shell membrane, again exhibiting mechanical robustness of the attachment observed.

The formation mechanism of the unique feature of the deflated nanospheres is proposed and illustrated in Figure 7. In
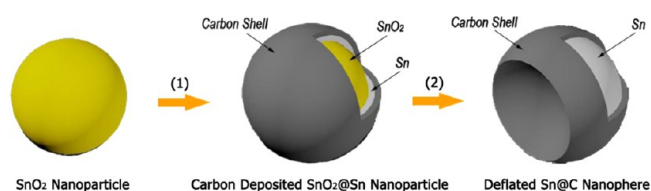

Figure 7. Illustration shows the plausible formation mechanism of the unique deflated nanosphere. Step 1: SnO_2 nanoparticle/aggregate was partially reduced forming a SnO_2@Sn@C particle with carbon deposition and encapsulation on the surface of initially. Step 2: Carbon shell shrinks after complete reduction of SnO_2 to metallic Sn with a volume reduction of the core forming a deflated Sn@C nanosphere.

the first step, under CVD conditions, acetylene could reduce the SnO_2 nanoparticle to metallic Sn starting from the surface of the solid SnO_2 nanoparticle generating a SnO_2@Sn particle. The melting point of SnO_2 of 1630 °C is much higher than the CVD temperature of 650 °C, while metallic Sn has a low melting point of 232 °C. The metallic Sn could simultaneously assist the catalytic decomposition of acetylene and have carbon from acetylene to deposit on the surface of the particle. Due to the low solubility of carbon in tin, the saturated carbon atoms would diffuse to the surface of the SnO_2@Sn nanoparticle forming a carbon shell. The solid SnO_2 nanoparticle provides a template to form a spherical carbon sheath without collapsing initially. Given the density difference between SnO_2 and Sn at 6.95 and 7.37 g/cm^3, respectively, the volume of the core particle would shrink upon complete reduction of SnO_2 to Sn inside the enclosed carbon sphere. The contraction stress exerted on the carbon sheath from the shrinkage of the core could lead to a deflated carbon sphere. Our current ongoing effort is to gain better understanding of the mechanism involved.

The as-prepared composite of deflated Sn@C nanospheres on 3-D carbonized walnut shell membranes was evaluated for reversible Na storage preliminarily (Figure 8). The first cycle discharge (Na insertion) capacity is about 260 mAh/g, and the first cycle charge (Na extraction) is about 163 mAh/g (Figure 8a). The first cycle irreversible capacity loss of 97 mAh/g could be attributed to the decomposition of the electrolyte to form a solid electrolyte interphase (SEI).[31,40] The plateau around 0.9 V in the first cycle discharge profile could be attributed to SEI
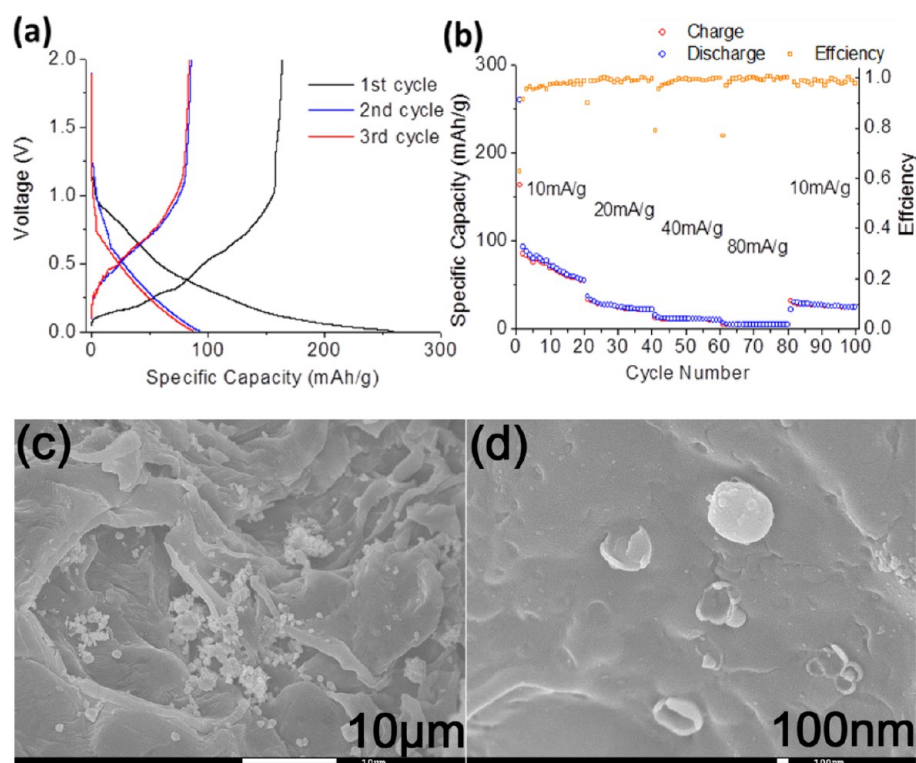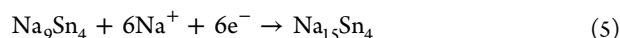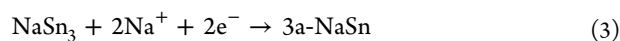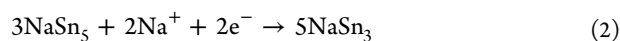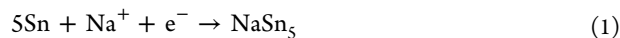
Figure 8. Preliminary evaluation of the unique deflated Sn@C nanospheres on 3-D layered carbon from biomass as a piece of material for reversible sodium ion storage: (a) first three cycle charge/discharge profiles and (b) cycling performance of 100 cycles under the current densities of 10, 20, 40, 80, and 10 mA/g and the Coulombic efficiency. FESEM images of the electrode after 100 cycles of test in sodium ion storage at (c) low-magnification overall view and (d) high-magnification showing broken carbon spheres.

formation. The subsequent plateaus around 0.5, 0.35, 0.15, and 0.1 V appeared upon further Na insertion, which could be assigned to the formation of $NaSn_5$, $NaSn$, Na_9Sn_4, and $Na_{15}Sn_4$, respectively.[31] The first cycle charge profile also exhibits multiple stage-like plateaus around 0.12, 0.25, 0.5, and 0.75 V, which could be assigned to the desodiation of $Na_{15}Sn_4$, Na_9Sn_4, $NaSn$, and $NaSn_5$, respectively.[31] To better interpret the date, the corresponding dQ/dV vs V was also plotted (Figure S6, Supporting Information). For the control without Sn at all, the dQ/dV vs V plots did not show any redox peaks associated with alloying and dealloying Sn and Na (Figure S6a in Supporting Information). The possible electrochemical reactions involved in different state of charge are[31,52]

$$5Sn + Na^+ + e^- \rightarrow NaSn_5 \quad (1)$$

$$3NaSn_5 + 2Na^+ + 2e^- \rightarrow 5NaSn_3 \quad (2)$$

$$NaSn_3 + 2Na^+ + 2e^- \rightarrow 3a\text{-}NaSn \quad (3)$$

$$4NaSn + 5Na^+ + 5e^- \rightarrow Na_9Sn_4 \quad (4)$$

$$Na_9Sn_4 + 6Na^+ + 6e^- \rightarrow Na_{15}Sn_4 \quad (5)$$

The plateaus also become weak from the second cycle onward. This dramatically reduce capacity from the first cycle to second cycle has not been observed in LIBs (Figure S7, Supporting Information), which will guarantee further studies. The cycling performance of the carbonization of walnut membranes with unique deflated Sn@C nanospheres in reversible sodium ion storage under the current rates of 10, 20, 40, 80, and 10 mA/g for 20 cycles each is shown in Figure 8b. Impressive high Coulombic efficiencies were achieved at different current rates, although the capacity drop was dramatic when the current rates increased. The capacity was not significant when the current rate was set at 80 mA/g. This observation could be attributed to slow solid-state diffusion kinetics with the large Na ionic size. Our current effort is to a develop rattle structure, where the tin core only takes a quarter of the space provided by the carbon nanospheres. One possible way to reduce the size of the core to a quarter is by controlled etching. In such a way, the additional space provided by the carbon shell will be enough to accommodate the 420% volumetric expansion of the reduced-sized tin core.

To better understand the mechanism of capacity fading, the composite electrode was evaluated after 100 cycles of SIB test. The low-magnification FESEM image of the electrode after the test (Figure 8c) suggests that the 3-D layered structures from walnut shell membranes were well preserved and could still affectively support the particles as before the cycling test. However, high-magnification FESEM (Figure 8d) showed that most of the nanospheres were broken with only the damaged carbon sheaths left, and many nanoparticles were peeled off from the layered carbon left multiple holes on the surface visible. There are still occasionally well-preserved particles, but the majority of the particles were damaged or peeled off. The observation could be used to explain the dramatic capacity drop discussed previously. Generally, less and less active Sn materials were available for reversible Na storage upon cycling leading to the capacity fading. It is also interesting to highlight that the observations after 100 cycles of the test also revealed two pieces of important information: (1) The carbon spheres were indeed well attached on the surface of the layered carbon. In fact, the carbon spheres were partially immersed into the near surface. This could be used to explain the mechanical robustness of the

attachment. (2) The broken carbon sheaths suggest that electrochemical sodium ion insertion could be adopted as "scissors" to cut nanospheres at large scale. The second part is being actively explored in our group currently.[53] In comparison, no broken nanospheres were observed in the same composite after being cycled in LIBs (Figure S8, Supporting Information). As one may note, we have selected higher currents in our testing of LIBs as compared to SIBs. The difference was mainly determined by our understanding of the ionic radii of Na^+ and Li^+ at 59 and 102 pm, respectively.[54] The actual ionic radii are also dependent the ionic coordinations. Compared to lithium ions, the sodium ions have much slower solid-state diffusion kinetics, and the Na-insertion/extraction reactions have much poorer reaction kinetics than that of Li-insertion/extraction reactions.[55] Therefore, to fully assess the sodium storage capacity of the active materials, the testing current is typically set at a much smaller number than that used in lithium ion batteries. The difference could be attributed to less volume variation involved in LIBs as compared to SIBs. Consequently, the better stability of the Sn@C composite electrode in LIBs than that of SIBs could be the reason for superior electrochemical performances of the former.

■ CONCLUSIONS

The novel preparation of deflated Sn@C nanospheres on 3-D layered carbon from carbonized walnut shell membranes is reported. The *in situ* reduction of SnO_2 to metallic Sn and the encapsulation of Sn particles by carbon spheres under CVD conditions can form stable deflated Sn@C nanospheres on the surface of layered carbon. It is interesting to highlight that all the carbon spheres encapsulating Sn particles are deflated, which could provide extra space for Sn to expand. The Sn@C deflated spheres are uniformly distributed on the 3-D structure of the carbonized walnut shell membranes, and the composite as a piece of material is a ready electrode that can be directly assembled into testing cells without any further treatment. Impressive high Coulombic efficiencies were achieved at different rates in SIBs. We observed significant differences in electrochemical performances of the as-prepared composite in reversible storage of Na and Li. Sn@C nanospheres would be broken in SIBs but well preserved in LIBs. This observation suggests the importance of the ionic size of Li and Na and the effect on the electrode materials during cycling. Different from application requirements in LIBs, SIBs will require extra space for Sn to expand inside the hollow carbon nanospheres, or rattle structure, in order to maintain a good cycling performance, which is our on-gong effort.

■ ASSOCIATED CONTENT

ⓈSupporting Information

Images of walnut shell membrane, TGA of the Sn@C composite, sample obtained at different conditions, first cycle dQ/dV vs V plot, performance in LIBs, and FESEM images of the composite after cycled in LIBs. This material is available free of charge via the Internet at http://pubs.acs.org.

■ AUTHOR INFORMATION

Corresponding Author

*E-mail: da.deng@wayne.edu.

Notes

The authors declare no competing financial interest.

■ REFERENCES

(1) Levine, S. The great battery race. *Foreign Policy* **2010**, 88−95.

(2) Yoshino, A. The birth of the lithium-ion battery. *Angew. Chem., Int. Ed.* **2012**, *51*, 5798−5800.

(3) Palomares, V.; Serras, P.; Villaluenga, I.; Hueso, K. B.; Carretero-Gonzalez, J.; Rojo, T. Na-Ion batteries, recent advances and present challenges to become low cost energy storage systems. *Energy Environ. Sci.* **2012**, *5*, 5884−5901.

(4) Slater, M. D.; Kim, D.; Lee, E.; Johnson, C. S. Sodium-ion batteries. *Adv. Funct. Mater.* **2012**, DOI: 10.1002/adfm.201200691.

(5) Yabuuchi, N.; Kajiyama, M.; Iwatate, J.; Nishikawa, H.; Hitomi, S.; Okuyama, R.; Usui, R.; Yamada, Y.; Komaba, S. P2-type $Na_X[Fe_{1/2}Mn_{1/2}]O_2$ made from earth-abundant elements for rechargeable Na batteries. *Nat. Mater.* **2012**, *11*, 512−517.

(6) Ellis, B. L.; Makahnouk, W. R. M.; Makimura, Y.; Toghill, K.; Nazar, L. F. A multifunctional 3.5 V Iron-based phosphate cathode for rechargeable batteries. *Nat. Mater.* **2007**, *6*, 749−753.

(7) Hayashi, A.; Noi, K.; Sakuda, A.; Tatsumisago, M. Superionic glass-ceramic electrolytes for room-temperature rechargeable sodium batteries. *Nat. Commun.* **2012**, *3*, 856.

(8) Xiong, H.; Slater, M. D.; Balasubramanian, M.; Johnson, C. S.; Rajh, T. Amorphous TiO_2 nanotube anode for rechargeable sodium ion batteries. *J. Phys. Chem. Lett.* **2011**, *2*, 2560−2565.

(9) Stevens, D. A.; Dahn, J. R. High capacity anode materials for rechargeable sodium-ion batteries. *J. Electrochem. Soc.* **2000**, *147*, 1271−1273.

(10) Lu, X. C.; Xia, G. G.; Lemmon, J. P.; Yang, Z. G. Advanced materials for sodium-beta alumina batteries: Status, challenges and perspectives. *J. Power Sources* **2010**, *195*, 2431−2442.

(11) Slater, M. D.; Kim, D.; Lee, E.; Johnson, C. S. Sodium-ion batteries. *Adv. Funct Mater.* **2013**, *23*, 947−958.

(12) Pan, H. L.; Hu, Y. S.; Chen, L. Q. Room-temperature stationary sodium-ion batteries for large-scale electric energy storage. *Energ Environ. Sci.* **2013**, *6*, 2338−2360.

(13) Kim, S. W.; Seo, D. H.; Ma, X. H.; Ceder, G.; Kang, K. Electrode materials for rechargeable sodium-ion batteries: Potential alternatives to current lithium-ion batteries. *Adv. Energy Mater.* **2012**, *2*, 710−721.

(14) Lu, Y.; Zhang, S.; Li, Y.; Xue, L. G.; Xu, G. J.; Zhang, X. W. Preparation and characterization of carbon-coated $NaVPO_4F$ as cathode material for rechargeable sodium-ion batteries. *J. Power Sources* **2014**, *247*, 770−777.

(15) Ruffo, R.; Fathi, R.; Kim, D. J.; Jung, Y. H.; Mari, C. M.; Kim, D. K. Impedance analysis of $Na_{0.44}MnO_2$ positive electrode for reversible sodium batteries in organic electrolyte. *Electrochim. Acta* **2013**, *108*, 575−582.

(16) Takachi, M.; Matsuda, T.; Moritomo, Y. Cobalt hexacyanoferrate as cathode material for Na^+ secondary battery. *Appl. Phys. Express* **2013**, *6*, 025802.

(17) D'Arienzo, M.; Ruffo, R.; Scotti, R.; Morazzoni, F.; Maria, C. M.; Polizzi, S. Layered $Na_{0.71}COO_2$: A powerful candidate for viable and high performance Na-batteries. *Phys. Chem. Chem. Phys.* **2012**, *14*, 5945−5952.

(18) Lu, Y. H.; Wang, L.; Cheng, J. G.; Goodenough, J. B. Prussian Blue: A new framework of electrode materials for sodium batteries. *Chem. Commun.* **2012**, *48*, 6544−6546.

(19) Ge, P.; Fouletier, M. Electrochemical intercalation of sodium in graphite. *Solid State Ionics* **1988**, *28−30* (Part 2), 1172−1175.

(20) Wenzel, S.; Hara, T.; Janek, J.; Adelhelm, P. Room-temperature sodium-ion batteries: Improving the rate capability of carbon anode materials by templating strategies. *Energy Environ. Sci.* **2011**, *4*, 3342−3345.

(21) Cao, Y. L.; Xiao, L. F.; Sushko, M. L.; Wang, W.; Schwenzer, B.; Xiao, J.; Nie, Z. M.; Saraf, L. V.; Yang, Z. G.; Liu, J. Sodium ion insertion in hollow carbon nanowires for battery applications. *Nano Lett.* **2012**, *12*, 3783−3787.

(22) Shao, Y. Y.; Xiao, J.; Wang, W.; Engelhard, M.; Chen, X. L.; Nie, Z. M.; Gu, M.; Saraf, L. V.; Exarhos, G.; Zhang, J. G.; Liu, J. Surface-driven sodium ion energy storage in nanocellular carbon foams. *Nano Lett.* **2013**, *13*, 3909−3914.

(23) Qian, J. F.; Wu, X. Y.; Cao, Y. L.; Ai, X. P.; Yang, H. X. High capacity and rate capability of amorphous phosphorus for sodium ion batteries. *Angew. Chem., Int. Ed.* **2013**, *52*, 4633−4636.

(24) Kim, Y.; Park, Y.; Choi, A.; Choi, N. S.; Kim, J.; Lee, J.; Ryu, J. H.; Oh, S. M.; Lee, K. T. An amorphous red phosphorus/carbon composite as a promising anode material for sodium ion batteries. *Adv. Mater.* **2013**, *25*, 3045−3049.

(25) Hariharan, S.; Saravanan, K.; Ramar, V.; Balaya, P. A rationally designed dual role anode material for lithium-ion and sodium-ion batteries: Case study of eco-friendly Fe_3O_4. *Phys. Chem. Chem. Phys.* **2013**, *15*, 2945−2953.

(26) Bi, Z. H.; Paranthaman, M. P.; Menchhofer, P. A.; Dehoff, R. R.; Bridges, C. A.; Chi, M. F.; Guo, B. K.; Sun, X. G.; Dai, S. Self-organized amorphous TiO_2 nanotube arrays on porous Ti foam for rechargeable lithium and sodium ion batteries. *J. Power Sources* **2013**, *222*, 461−466.

(27) Zhu, H. L.; Jia, Z.; Chen, Y. C.; Weadock, N.; Wan, J. Y.; Vaaland, O.; Han, X. G.; Li, T.; Hu, L. B. Tin anode for sodium-ion batteries using natural wood fiber as a mechanical buffer and electrolyte reservoir. *Nano Lett.* **2013**, *13*, 3093−3100.

(28) Liu, Y. H.; Xu, Y. H.; Zhu, Y. J.; Culver, J. N.; Lundgren, C. A.; Xu, K.; Wang, C. S. Tin-coated viral nanoforests as sodium-ion battery anodes. *ACS Nano* **2013**, *7*, 3627−3634.

(29) Datta, M. K.; Epur, R.; Saha, P.; Kadakia, K.; Park, S. K.; Kuma, P. N. Tin and graphite based nanocomposites: Potential anode for sodium ion batteries. *J. Power Sources* **2013**, *225*, 316−322.

(30) Su, D. W.; Ahn, H. J.; Wang, G. X. SnO_2@graphene nanocomposites as anode materials for na-ion batteries with superior electrochemical performance. *Chem. Commun.* **2013**, *49*, 3131−3133.

(31) Xu, Y. H.; Zhu, Y. J.; Liu, Y. H.; Wang, C. S. Electrochemical performance of porous carbon/tin composite anodes for sodium-ion and lithium-ion batteries. *Adv. Energy Mater.* **2013**, *3*, 128−133.

(32) Huang, J. P.; Yuan, D. D.; Zhang, H. Z.; Cao, Y. L.; Li, G. R.; Yang, H. X.; Gao, X. P. Electrochemical sodium storage of $TiO_2(B)$ nanotubes for sodium ion batteries. *RSC Adv.* **2013**, *3*, 12593−12597.

(33) Wang, Y. X.; Lim, Y. G.; Park, M. S.; Chou, S. L.; Kim, J. H.; Liu, H. K.; Dou, S. X.; Kim, Y. J. Ultrafine SnO_2 nanoparticle loading onto reduced graphene oxide as anodes for sodium-ion batteries with superior rate and cycling performances. *J. Mater. Chem. A* **2014**, *2*, 529−534.

(34) Darwiche, A.; Sougrati, M. T.; Fraisse, B.; Stievano, L.; Monconduit, L. Facile synthesis and long cycle life of SnSb as negative electrode material for Na-ion batteries. *Electrochem. Commun.* **2013**, *32*, 18−21.

(35) Wang, Y.; Su, D. W.; Wang, C. Y.; Wang, G. X. SnO_2@MWCNT nanocomposite as a high capacity anode material for sodium-ion batteries. *Electrochem. Commun.* **2013**, *29*, 8−11.

(36) Su, D. W.; Wang, C. Y.; Ahn, H.; Wang, G. X. Octahedral tin dioxide nanocrystals as high capacity anode materials for Na-ion batteries. *Phys. Chem. Chem. Phys.* **2013**, *15*, 12543−12550.

(37) Gonzalez, J. R.; Nacimiento, F.; Alcantara, R.; Ortiz, G. F.; Tirado, J. L. Electrodeposited $CoSn_2$ on nickel open-cell foam: Advancing towards high power lithium ion and sodium ion batteries. *CrystEngComm* **2013**, *15*, 9196−9202.

(38) Wang, J. W.; Liu, X. H.; Mao, S. X.; Huang, J. Y. Microstructural evolution of Tin nanoparticles during in situ sodium insertion and extraction. *Nano Lett.* **2012**, *12*, 5897−5902.

(39) Zhou, X. S.; Bao, J. C.; Dai, Z. H.; Guo, Y. G. Tin nanoparticles impregnated in nitrogen-doped graphene for lithium-ion battery anodes. *J. Phys. Chem. C* **2013**, *117*, 25367−25373.

(40) Xiao, L. F.; Cao, Y. L.; Xiao, J.; Wang, W.; Kovarik, L.; Nie, Z. M.; Liu, J. High capacity, reversible alloying reactions in SnSb/C nanocomposites for Na-ion battery applications. *Chem. Commun.* **2012**, *48*, 3321−3323.

(41) Ming, J.; Wu, Y. Q.; Liang, G. F.; Park, J. B.; Zhao, F. Y.; Sun, Y. K. Sodium salt effect on hydrothermal carbonization of biomass: A catalyst for carbon-based nanostructured materials for lithium-ion battery applications. *Green Chem.* **2013**, *15*, 2722−2726.

(42) Unur, E. Functional nanoporous carbons from hydrothermally treated biomass for environmental purification. *Microporous Meso-porous Mater.* **2013**, *168*, 92−101.

(43) Wang, X. Y.; Wang, H. Q.; Dai, Q. F.; Li, Q. Y.; Yang, J. H.; Zhang, A. N.; Yan, Z. X. Preparation of novel porous carbon spheres from corn starch. *Colloids Surf., A* **2009**, *346*, 213−215.

(44) Li, Q.; Yuan, X. D.; Zeng, G. F.; Xi, S. Q. Study on the microstructure and properties of nanosized stannic oxide powders. *Mater. Chem. Phys.* **1997**, *47*, 239−245.

(45) Deng, D.; Lee, J. Y. A family of aligned C-curved nanoarches. *ACS Nano* **2009**, *3*, 1723−1728.

(46) Deng, D.; Lee, J. Y. Reversible storage of lithium in a rambutan-like tin-carbon electrode. *Angew. Chem., Int. Ed.* **2009**, *48*, 1660−1663.

(47) Deng, D.; Lee, J. Y. Direct fabrication of double-rough chestnut-like multifunctional Sn@C composites on copper foil: Lotus effect and lithium ion storage properties. *J. Mater. Chem.* **2010**, *20*, 8045−8049.

(48) Sharma, R. K.; Wooten, J. B.; Baliga, V. L.; Martoglio-Smith, P. A.; Hajaligol, M. R. Characterization of char from the pyrolysis of tobacco. *J. Agric. Food Chem.* **2002**, *50*, 771−783.

(49) Ni, W.; Wang, Y. B.; Xu, R. Formation of Sn@C yolk-shell nanospheres and core-sheath nanowires for highly reversible lithium storage. *Part. Part. Syst. Charact.* **2013**, *30*, 873−880.

(50) Jankovic, L.; Gournis, D.; Trikalitis, P. N.; Arfaoui, I.; Cren, T.; Rudolf, P.; Sage, M. H.; Palstra, T. T. M.; Kooi, B.; De Hosson, J.; Karakassides, M. A.; Dimos, K.; Moukarika, A.; Bakas, T. Carbon nanotubes encapsulating superconducting single-crystalline tin nano-wires. *Nano Lett.* **2006**, *6*, 1131−1135.

(51) Sveningsson, M.; Morjan, R. E.; Nerushev, O. A.; Sato, Y.; Bäckström, J.; Campbell, E. E. B.; Rohmund, F. Raman spectroscopy and field-emission properties of CVD-grown carbon-nanotube films. *Appl. Phys. A: Mater. Sci. Process.* **2001**, *73*, 409−418.

(52) Ellis, L. D.; Hatchard, T. D.; Obrovac, M. N. Reversible insertion of sodium in tin. *J. Electrochem. Soc.* **2012**, *159*, A1801−A1805.

(53) Chen, W.; Deng, D. Sodium-cutting: A new top-down approach to cut open nanostructures on nonplanar surfaces on a large scale. *Chem. Commun.* **2014**, *50*, 13327−13330.

(54) Atkins, P. De Paula, J. *Atkins' Physical Chemistry*; W.H. Freeman: New York, 2006.

(55) Zhu, Y. J.; Xu, Y. H.; Liu, Y. H.; Luo, C.; Wang, C. S. Comparison of electrochemical performances of olivine $NaFePO_4$ in sodium-ion batteries and olivine $LiFePO_4$ in lithium-ion batteries. *Nanoscale* **2013**, *5*, 780−787.